Colloidal Stability of PFSA-Ionomer Dispersions

Part I: Single-Ion Electrostatic Interaction Potential Energies

Harsh Srivastav[1,2], Adam Z. Weber[2], and Clayton J. Radke*[,1]

[1]Department of Chemical and Biomolecular Engineering,
University of California, Berkeley, 201 Gilman, South Dr., CA 94720

[2]Energy Technologies Area,

Lawrence Berkeley National Laboratory, Building 30, Cyclotron Road, Berkeley, CA 94720

*Corresponding author: Clayton Radke, radke@berkeley.edu

Abstract

Charged colloidal particles neutralized by a single counterion are increasingly important for many emerging technologies. Attention here is addressed specifically to hydrogen fuel cells and water electrolyzers whose catalyst layers are manufactured from perfluorinated sulfonic acid polymer (PFSA) suspended in aqueous/alcohol solutions. Partially dissolved PFSA aggregates, known collectively as ionomer, are stabilized by the electrostatic repulsion of overlapping diffuse double layers consisting only of protons dissociated from the suspended polymer. We denote such double layers containing no added electrolyte as "single ion". Size-distribution predictions build upon interparticle interaction potential energies from the Derjaguin-Landau-Verwey-Overbeek (DLVO) formalism. However, when only a single counterion is present in solution, classical DLVO electrostatic potential energies no longer apply. Accordingly, here a new formulation is proposed to describe how single-counterion diffuse double layers interact in colloidal suspensions. Part II of this contribution uses the new single-ion interaction energies to predict aggregated size distributions and resulting solution pH of PFSA in mixtures of n-propanol and water.

A single-counterion diffuse layer cannot reach an electrically neutral concentration far away from a charged particle. Consequently, nowhere in the dispersion is the solvent neutral, and the diffuse layer emanating from one particle always experiences the presence of other particles (or walls). Thus, in addition to an intervening interparticle repulsive force, a back-side osmotic force

is always present. With this new construction, we establish that single-ion repulsive pair-interaction energies are much larger than classical DLVO electrostatic potentials. The proposed single-ion electrostatic pair potential governs dramatic new dispersion behavior including dispersions that are stable at low volume fraction but unstable at high volume fraction and finite volume-fraction dispersions that are unstable with fine particles but stable with coarse particles. The proposed single-counterion electrostatic pair potential provides a general expression to predict colloidal behavior for any charged-particle dispersion in ionizing solvents with no-added-electrolyte.

Introduction

Proton-Exchange-Membrane Fuel Cells offer a promising replacement to traditional combustion engines that have deleterious emissions. The catalyst layers of these cells are currently produced via ink fabrication and deposition involving empirically formulated colloidal dispersions of perfluorinated sulfonic-acid polymer (PFSA) and other ionomers.[1–4] Colloidal dispersions are commonly assumed to be stable when the total interparticle potential-energy maximum is more than a few $k_B T$ units, where k_B is Boltzmann's constant and T is absolute temperature.[5–7] When the potential-energy maximum is less than this value or is everywhere negative, the dispersion is unstable and particles aggregate.[5,6,8,9] Aggregation kinetics in a quiescent dispersion often follows perikinetic Smoluchowski kinetics that depend strongly on the pairwise interaction energies between particles.[5,6,8,9]. For electrostatically stabilized charged particle dispersions in electrolyte-supporting solvents, the pairwise interaction potential traditionally consists of a Hamaker attractive interaction and a repulsive electrostatic interaction (*i.e.*, so-called DLVO theory).[5–11] The electrostatic pair potential originates from overlap of diffuse double layers encompassing two charged interacting particles. When the opposing particles separate significantly beyond the Debye length, the intervening solution is electrically neutral. Added positive and negative electrolyte ions allow electroneutrality to extend to distances infinitely far away where the electrostatic potential reaches a reference constant, normally taken to be zero.[5,7,9,12–16]

However, in dispersions where the particle charge arises from surface-ion dissociation/desorption and no electrolyte is added to the solvent, only released counterions neutralize the remnant surface charge. For fuel cells and water electrolyzers,[8,17–24] surface charge of the PFSA aggregates arises from dissociation of sulfonic-acid side groups with pK_As near -6 in

water.[17] Overall electroneutrality then demands that nowhere in the solution is there electrical neutrality. Suspended particles constantly feel the presence of other nearby particles. With no background electrolyte, the effective Debye length then depends on the presence of nearby particles, and, hence, strongly on the colloidal volume fraction. Modeling a diffuse double layer where only counterions are present requires more care as the counterions cannot migrate infinitely far away into a neutral solvent (or into a neutral $\mathrm{pH} = 7$ aqueous solvent).[7,13] Due to lack of far-field electroneutrality, a single-counterion diffuse layer cannot reach a uniform concentration far away from a charged particle, including a zero concentration. Rather, the diffuse layer encompassing one particle continually interacts with those emanating from other close-by charged particles (or walls). As single counterions migrate away from the charged surface the entire volume of the dispersion medium is occupied by non-neutral diffuse double layers.

Some previous effort has focused on electrostatic interaction energies with single-counterion diffuse layers.[5] Cowley derived the single-ion concentration profile between two phospholipid layers to obtain the force between the layers.[13] Engstrom and Wennerstrom utilized no-added electrolyte theory to analyze lyotropic liquid crystals. Using an assumed double-layer length, the fraction of adsorbed and free counterions in solution was obtained.[25] Eventually, the no-added electrolyte case garnered interest as a theoretical consideration of itself.[7,16] There are important examples, however, of single-counterion colloid dispersions. These works on single-counterion diffuse-layer overlap impose a zero-ion concentration everywhere except in the intervening space between the particles. Consequently, these works do not establish electrostatic pair potentials appropriate to colloidal suspensions.

Equal-size particle-particle interactions for single counterions are inherent in Wigner-Seitz cells, where the solvent is partitioned around each particle, but these largely consider static spatially organized particles. Alexander et. al obtained integral expressions for solving the potential distributions for charge-neutralized Wigner-Seitz cells using the linearized Poisson-Boltzmann equation.[26] Bocquet et. al and Ryoo et. al both numerically solve the nonlinear equation for spherical cells, using constant potential boundary conditions as a proxy for constant charge.[27,28] Sengupta and Papadopoulos consider the role of particle volume fraction in van der Waal forces.[29] Unfortunately, none of these works establish single-ion electrostatic interaction potentials as a

function of separation distance for a pair of mobile or colliding particles in a fixed volume-fraction suspension.

Wigner-Seitz cells also permit calculation of electrostatic interactions in periodic colloid crystals where the intervening spacing between the particles is non-neutral everywhere.[30–35] It is important to realize, however, that calculations undergirding colloidal crystals utilize classical added-electrolyte theory. As the lattice spacing of the crystal increases asymptotically and the suspension volume fraction diminishes towards zero, the intervening liquid becomes electrically neutral with a well-defined bulk Debye length. This case contrasts with single-ion diffuse double layers where very dilute suspensions asymptotically reach zero ionic strength in the intervening liquid with no well-defined bulk Debye length. Single-ion double layer systems are more complicated than colloidal crystals, as outlined below. In classical added-electrolyte suspensions, surface dissociation of single counterions commonly is present but minimally contributes compared to the added electrolyte and is traditionally neglected.[5,7,9]

With no added electrolyte, the effective Debye length depends on the presence of nearby particles even for a dilute dispersion making the interaction pair potential a function of suspension volume fraction. Our work here in Part I thus deviates substantially from prior efforts[7,13–16,31–34] by considering the effect of the diffuse double layers emanating from surrounding particles on the pair interaction energy. Nearby diffuse double layers provide a background osmotic force on the interacting particle pair. Lack of this backside-electrolyte osmotic pressure leads to unrealistically large electrostatic repulsion, as in the previous efforts above. Because single-ion diffuse layers continually interact with other particles in the dispersion, we relieve the zero-background ion-concentration approximation. A new closed-form relation is presented for the repulsive electrostatic interaction energy in dispersions with no-added electrolyte. As opposed to classical double-layer theory with an indifferent electrolyte present, the no-added electrolyte interaction pair potential is multibody in that it depends on the volume fraction of the suspended particles. In the next section, overlapping single-counterion diffuse layers are analyzed and extended to predict electrostatic pair-interaction forces. Finally, we compare to classical theories and explain observed significant deviations.

Theory

Upon immersion of dry ion-exchange colloidal particles, soluble counterions dissociate/desorb from surface exchange sites into solution and neutralize the remnant surface charge. For example, in the case of anionic-exchange particles, exchangeable cations release into solution. Figure 1A illustrates the case of anionic ionogenic particles in water with only cations dissociating into solution to provide overall neutrality for each particle in the suspension. In classical diffuse double-layer theory, however, electrolyte is added to the polar liquid; particle-desorbed ions are traditionally neglected in comparison to the background electrolyte. Figure 1B illustrates this case. With added electrolyte, each particle is neutralized by a diffuse double layer that achieves neutrality when extended beyond several Debye lengths. Not so in Figure 1A for a single-counterion double layer. When there is no or very dilute added electrolyte, the solution ion cloud is no longer electrically neutral far from the particle.

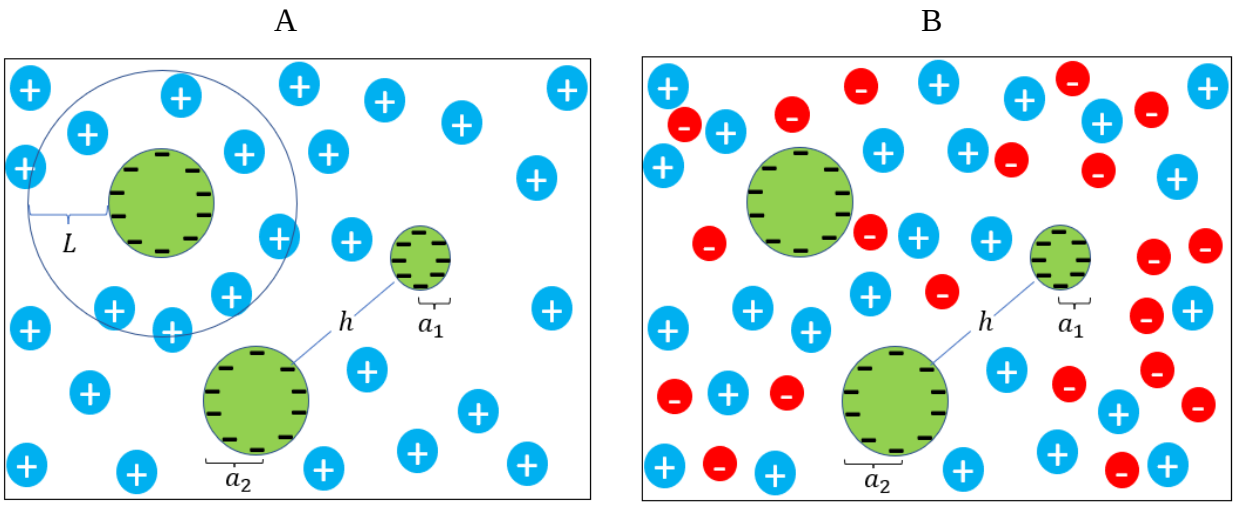

Figure 1: Schematic of anionic spherical colloidal particles of radii a_1 and a_2 in a liquid dispersion characterized by an average separation distance of h. A. Anionic particles are neutralized by a single cation. The extent of the neutralizing diffuse double layer is denoted by L. B. Anionic particles are neutralized by an electrolyte with both anions and cations that reach electroneutrality far from the particles.

To address the general single-counterion problem, we consider a colloidal dispersion of unequal-size spheres with cation-exchange sites and immersed in a polar solvent with no added electrolyte (the case of anion-exchange sites follows by direct analogy). Following others,[7,13–16,25] the Poisson-Boltzmann equilibrium relation provides an exact solution for zero-added-electrolyte

diffuse double layers for flat plates. We then utilize the Derjaguin approximation[7,13,16,36] to extend the flat-plate pairwise electrostatic interaction to interacting spheres.

Consider first a single, isolated flat plate in the presence of an added indifferent electrolyte, which applies in determining the backside repulsion of each particle. The classical Poisson-Boltzmann equation is solved subject to two boundary conditions:

$$\Phi(x \to \infty) = 0 \tag{1}$$

and Gauss's law,

$$\Phi'(\mathrm{x} = 0) = -\frac{q}{\epsilon} \tag{2}$$

where x is the distance from the charged surface, q is the surface charge density, ϵ is the solution dielectric permeability, and Φ is the electrostatic potential. Implicit in the mathematical solution is the idea that if $\Phi \to 0$ monotonically as $x \to \infty$, then all derivatives of Φ similarly approach zero as $x \to \infty$.

For ionogenic particles submerged in an electrolyte-free solvent, the counterions released from the surface cannot be ignored. When only a single counterion surrounds the charged surface, the Poisson-Boltzmann equation is

$$\frac{\mathrm{d}^2\Phi}{dx^2} = -\frac{zeC_\infty}{\epsilon}\exp\left(-\frac{ze\Phi}{k_BT}\right) \tag{3}$$

where e is the charge of an electron, R is the ideal gas constant, T is absolute temperature, and z and C_∞ are the charge number and number concentration of counterions far from the surface, respectively, which must be non-zero for a solution-charge distribution to exist. At a very large distance, the electrostatic potential and all of its derivatives are zero everywhere, while the right side of Equation 3 approaches a non-zero constant. Equation 1, therefore, is not an applicable boundary condition. Accordingly, counterions dissociating/desorbing from the particle surface must be located within a finite distance away from the surface, L, *i.e.*, the extent of the spatial charge distribution in solution. Figure 1A depicts schematically the meaning of overlap distance, L. When the solvent is water, dissociation demands an electrically neutral region as the pH approaches 7 far from a particle. However, we demonstrate later in Results and Discussion that this rarely occurs for realistic suspension volume fractions. pH equilibrium is thus ignored in further analysis.

To address single-counterion particle neutralization in Figure 1A, we take the characteristic double-layer overlap distance, L, as a reference. Poisson-Boltzmann theory for a single counterion then reads

$$\frac{\mathrm{d}^2\Phi}{dx^2} = -\frac{zeC_L}{\epsilon}\exp\left(-\frac{ze\Phi}{k_BT}\right) \tag{4}$$

with boundary conditions

$$\Phi(L) = 0 \tag{5}$$

and

$$\Phi'(0) = -\frac{q}{\epsilon} \tag{6}$$

where C_L denotes the molecular concentration of counterions at L. At this juncture, L is unspecified. Electroneutrality constrains the derivative of Φ at $x = L$, as

$$q = -ze\int_0^L C(x)\,dx = \epsilon\int_0^L \frac{d^2\Phi}{dx^2}\,dx = -\epsilon\left[\left.\frac{d\Phi}{dx}\right|_{x=0} - \left.\frac{d\Phi}{dx}\right|_{x=L}\right] \tag{7}$$

For finite L and from Equation 6, this result implies that $\Phi'(L) = 0$ in addition to $\Phi(L) = 0$. Equations 4-6 are then solved to yield[7,13–16,25,37–39]

$$\Phi = \frac{k_BT}{ze}\ln\left(\cos^2\left(\frac{x-L}{\lambda_L\sqrt{2}}\right)\right) \tag{8}$$

with a surface charge density of

$$q = -\mathrm{sign}(z)\sqrt{2\epsilon RTC_L}\tan\left(\frac{L}{\lambda_L\sqrt{2}}\right) \tag{9}$$

and an effective Debye length of

$$\lambda_{\mathrm{L}}^2 = \frac{\epsilon k_BT}{z^2e^2C_L} \tag{10}$$

Although defined analogously to the traditional Debye length, C_L appearing in Equation 10 is that corresponding to the overlap concentration and not that of a bulk electrically neutral solution. Given the surface charge density, q, and the characteristic double-layer dimension, L, discussed below, Equation 9 is solved numerically to specify C_L. For L approaching infinity, C_L approaches zero and the Debye length approaches infinity meaning that the double layer extends very far from the

surface. Later, we wish an expression for the average counterion concentration, $\langle C \rangle$, in the single-ion double layer, which is determined from Equations 7 and 9,

$$\langle C \rangle = -\frac{q}{zeL} = \frac{\sqrt{2\epsilon k_B T C_L}}{|z|eL} \tan\left(L\sqrt{\frac{z^2 e^2 C_L}{2\epsilon RT}} \right) = C_L \left(\frac{\lambda_L \sqrt{2}}{L} \right) \tan\left(\frac{L}{\lambda_L \sqrt{2}} \right) \tag{11}$$

One immediate consequence of Equation 11 is that for a fixed surface charge density, the product $L\sqrt{C_L}$ approaches a constant as L grows large. Indeed, because the argument for the tangent function is bounded, for large L one obtains

$$L\sqrt{\frac{z^2 e^2 C_L}{2\epsilon k_B T}} = \frac{L}{\lambda_L \sqrt{2}} = \frac{\pi}{2}, L \to \infty \tag{12}$$

Thus, for an infinite extent of the double layer, the counterion concentration approaches zero asymptotically, but the product $L\sqrt{C_L}$ remains constant.

To proceed, we formulate the repulsive electrostatic potential energy between two interacting charged flat plates separated by a distance h with molecular single-ion concentration C_m at the midplane. The Poisson-Boltzmann relation for the single counterion distribution between two flat plates becomes

$$\frac{\mathrm{d}^2\Phi}{dx^2} = -\frac{zeC_m}{\epsilon} \exp\left(-\frac{ze(\Phi - \Phi_\mathrm{m})}{k_B T} \right) \tag{13}$$

where the origin of x is at the midplane of potential, Φ_m, between the plates. Boundary conditions for Equation 13 are symmetry at the midplane, $\Phi'(0) = 0$, and Gauss' law at the surface of either plate: $\Phi'\left(-\frac{h}{2}\right) = -\frac{q}{\epsilon}$. With these boundary conditions, the analytic solution to Equation 13 is

$$\Phi - \Phi_m = \frac{k_B T}{ze} \ln\left(\cos^2\left(\frac{x}{\lambda_m \sqrt{2}} \right) \right) \tag{14}$$

where the Debye length is now based on the midplane concentration,

$$\lambda_m^2 = \frac{\epsilon k_B T}{z^2 e^2 C_m} \tag{15}$$

Similar to the single-plate case in Equation 9 above, the midplane ion concentration is determined numerically from the surface charge density on each plate for each separation distance,

$$q = -\text{sign}(z)\sqrt{2\epsilon k_B T C_m}\tan\left(\frac{\frac{h}{2}}{\lambda_m\sqrt{2}}\right) = -\text{sign}(z)\sqrt{2\epsilon k_B T C_m(h)}\tan\left(\frac{h}{2}\sqrt{\frac{z^2e^2C_m(h)}{2\epsilon k_B T}}\right) \quad (16)$$

To establish the flat-plate pair interaction potential, we first write the difference in osmotic pressures on each plate to give the repulsive electrostatic force per unit area as [5,7,9]

$$P(h) = k_B T[C_m(h) - C_L] \quad (17)$$

The background concentration used here, C_L , assumes that pairwise forces cancel upon reaching a separation distance of $2L$ after which the double layers no longer interact (*i.e.*, the electrostatic repulsive force remains in effect only out to a distance of $2L$).

Previous literature neglected the osmotic pressure acting on the exterior of each plate[7,14–16,36,40], thus demanding that C_L equals zero and that the midplane Debye length extends to infinity. Interacting particle pairs are thus isolated and immersed in an infinite solvent bath. In a dispersion, however, each particle is surrounded by others and interacts with the extended double layers from surrounding particles (see Figure 1). Thus, the osmotic pressure exerted by counterions extending out to L should not be neglected even at small particle volume fractions.

Given the particle surface charge, the repulsive energy per unit area (V_R) between two flat plates is[5,7,9]

$$V_R(h) = \int_h^{2L} P(x)\,dx \quad (18)$$

where $P(x)$ follows from Equation 17. As noted above, the Derjaguin approximation transforms the flat-plate expression to that between two spheres of radii a_1 and a_2 with equal surface charge densities[41], yielding the expression

$$U_r(h) = \frac{2\pi a_1 a_2}{a_1 + a_2}\int_h^{2L} V_R(y)\,dy = \frac{2\pi a_1 a_2}{a_1 + a_2}k_B T\int_h^{2L}\int_y^{2L}(C_m(x) - C_L)\,dxdy \quad (19)$$

for the electrostatic interaction energy, $U_r(h)$, where y is the local flat-plate surface separation distance varying along the sphere surface in the Derjaguin approximation and h is the surface separation distance along the common radius. This energy reflects the net potential-of-mean-force repulsion between two spheres at a surface separation distance h relative to a separation distance of $2L$ where the net force on the interacting spheres is zero. Because of the presence of other particles

at L in the pair-potential calculation, $U_r(h)$ is explicitly multibody. The integrand in the last equality does not depend on the sizes of the two spheres and can be further simplified by a change in the order of integration to

$$U_r(h) = \frac{2\pi a_1 a_2}{a_1 + a_2} k_B T \int_h^{2L} (y - h)(C_m(y) - C_L)\, dy \tag{20}$$

Equation 20 is numerically integrated once $C_m(y)$ is specified from Equation 16 for discrete-distance increments in the interval $h \leq y \leq L$, and C_L is established from Equation 9. Details are given in SI. Several approximations are inherent in Eqn. 20. First, the Derjaguin framework is most accurate at small distances compared to particle size. Second, we neglect finite ion-size effects, mostly because ion concentrations are low in our experimental effort of Part II. Third, we treat aggregated particles as effective spheres. Each of these approximations is also inherent in the added-electrolyte case. Still, Equation 20 provides a powerful tool to compute repulsive energies in suspensions with and without an added electrolyte."

Importantly, knowledge of L is necessary to evaluate Equation 20. Here, L is taken as a measure of the average separation distance between suspended particles that depends on the volume fraction of particles φ. Averaging the void space around each sphere yields[9]

$$\frac{L}{a} = \frac{1}{\phi^{\frac{1}{3}}} - 1 \tag{21}$$

where a is an average spherical particle radius. Once L is specified, Equation 9 gives C_L, and, hence, the effective Debye length, λ_L. Note that Equation 21 makes the electrostatic potential energy multibody in the sense that the effective Debye length is a function of particle volume fraction.

If C_L is neglected in Equations 19 and 20, leading to no external particle osmotic-interaction force [7], we obtain

$$U_r(h) = \frac{2\pi a_1 a_2}{a_1 + a_2} k_B T \int_h^{\infty} (y - h) C_m(y)\, dy, \qquad C_L = 0 \tag{22}$$

In this case, C_m is a function only of q and h, but not of L, so the electrostatic repulsive energy no longer depends on how concentrated or dilute is the dispersion. Numerical methodology to quantify $U_r(h)$ is outlined in SI.

Equations 20 and 22 allow comparison between the finite and zero volume-fraction dispersions with no added electrolytes, respectively. It is also helpful to compare with the classical added-electrolyte case. Counterions dissociated/desorbed from the dry neutral dispersion particles in the added-electrolyte case are traditionally ignored in comparison to the concentration of added indifferent electrolyte. As noted below, at very dilute background electrolyte, corresponding, for example, to the lowest possible concentration reflecting neutral-pH water, the released-ion contribution to the diffuse layer is negligible except at extremely low particle volume fractions. For an added z:z electrolyte, the classic Poisson-Boltzmann equation is solved between two flat plates and for a single isolated plate with the boundary conditions listed in Equations 1 and 2 for the no-added electrolyte cases with L approaching infinity. The net osmotic-pressure force on the interacting plates is now given by[5,7,9]

$$P(h) = k_B T\left[\left(C_{m+}(h) - C_{+,\infty}\right) + \left(C_{m-}(h) - C_{-,\infty}\right)\right] = 2k_B T C_\infty \left[\cosh\left(\frac{ze\Phi_m}{k_B T}\right) - 1\right] \quad (23)$$

The expression for the flat-plate interaction potential remains the same as in Equation 18 but with the integral upper bound changed to infinity. Finally, the repulsive interaction pair-potential energy between two spheres with the Derjaguin approximation follows as above after change of integration order:

$$U_r(h) = \frac{4\pi a_1 a_2}{a_1 + a_2} k_B T C_\infty \int_h^\infty (y - h)\left(\cosh\left(\frac{ze\Phi_m(y)}{k_B T}\right) - 1\right) dy \quad (24)$$

As with the no-added electrolyte case in Equation 20, Equation 24[42] requires numerical integration after the Poisson-Boltzmann equation is solved numerically.

It is useful to compare the linearized formulations of the added and no-added electrolyte cases because the linearized approximation is often used in practice. Details of their derivation are presented in SI. In the comparison calculations below, parameters are for monodisperse spheres of uniform radius $a = 25$ nm and surface charge density $q = -0.1\ \mathrm{C/m^2}$ (*i.e.*, one anionic charged surface group per 1.62 nm^2) suspended in a solvent of $\epsilon/\epsilon_0 = 80$ at $T = 25$℃, unless otherwise noted. For reference, charge densities for silica reach about $-0.1\ \mathrm{C/m^2}$ at a pH of 7.5 with a RbCl concentration of 0.05 M.[43] The surface charge density for Nafion™ PFSA in Part II[44] is $-0.214\ \mathrm{C/m^2}$, close to the example charge density assumed here. The suspension concentration is varied to cover a large particle volume-fraction range ($\phi = 0.001$ to $\phi = 0.5$).

Results and Discussion

Figure 2 presents a main result of this work: the repulsive single-counterion dimensionless electrostatic pair-potential energy as a function of separation distance for four particle volume fractions. As opposed the to the classical added-electrolyte case, electrostatic potential energies asymptotically vanish when $h = 2L$. The lowest volume fraction of $\phi = 0.001$ and below approaches $C_L = 0$ as in Equation 22 or, equivalently, approaching a zero volume-fraction dispersion. Note the very large repulsive energies that arise in this case. When the effect of dispersion-finite volume fraction is accounted for in Equations 20 and 21, however, potential energies dramatically reduce. Consequently, unless the effect of finite particle concentration is considered, all no-added electrolyte dispersions should remain electrostatically stable and not aggregate in contradiction to reported experimental results.[8,18,19,21,45] Conversely, stable dispersions of low volume fraction can become unstable at higher at higher particle volume fractions. Neither of these results arise in classical added-electrolyte interaction-potential theory.[5–7,9]

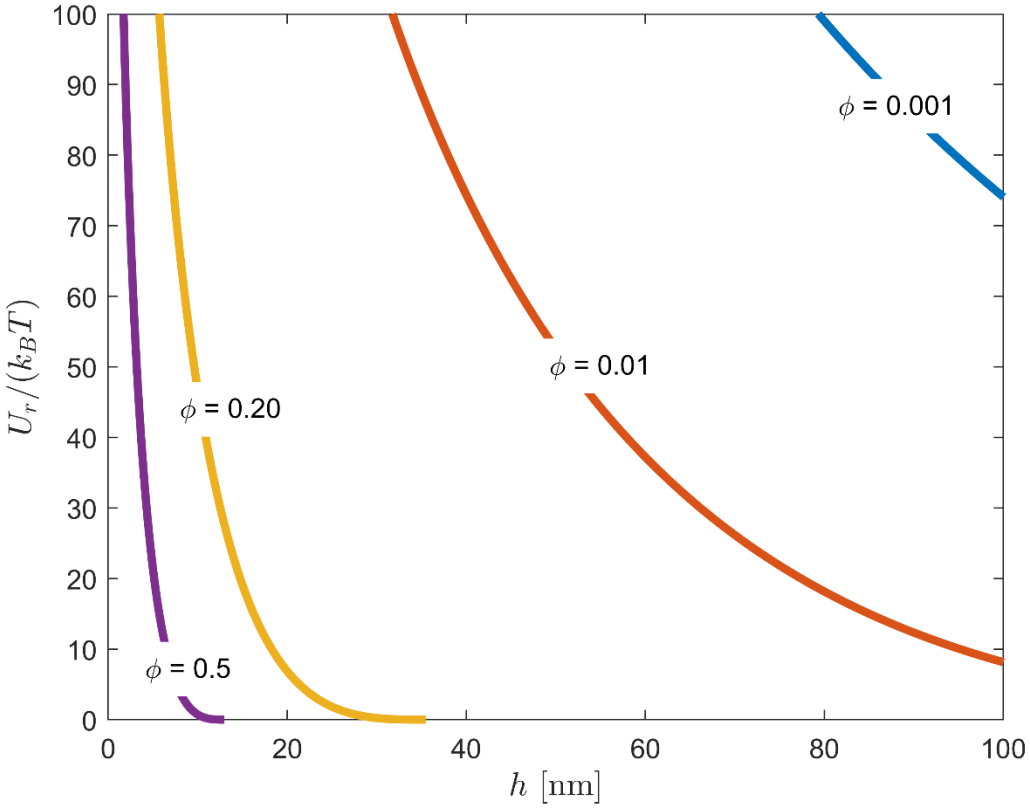

Figure 2: Normalized single-counterion repulsive electrostatic interaction energy between two equal-sized spheres ($a = 25$ nm) as a function of separation distance for varying volume fraction. A volume fraction of $\phi = 0.001$ approaches the dilute limit representing no backside repulsion (*i.e.*, $\mathrm{L} \to \infty$). $q = -0.1\ \mathrm{C/m^2}$.

The role played by particle size on the single-counterion electrostatic potential is twofold. First for equal-sized particles, the integral pre-factor in Equation 20 demands a linear increase of $U_r(h)$ with increasing spherical radius similar to added-electrolyte theory. More subtly, there is a second role of a from Equation 21: for a given particle volume fraction, larger particles begin to interact out to larger double-layer extents. Accordingly, larger sized spheres evoke magnified electrostatic repulsion and vice versa, effects not seen in the added-electrolyte overlapping diffuse double layers. Figure 3 displays this second effect by graphing the integral in Equation 20 (*i.e.*, $U_r(h)/\pi a k_B T$) versus h for a fixed particle volume fraction of $\phi = 0.5$ and for various sphere radii. Thus, no-added electrolyte colloidal dispersions exhibit much stronger increases in electrostatic repulsion with increasing particle size than do added-electrolyte dispersions, where all lines in Figure 3 collapse onto a single curve.

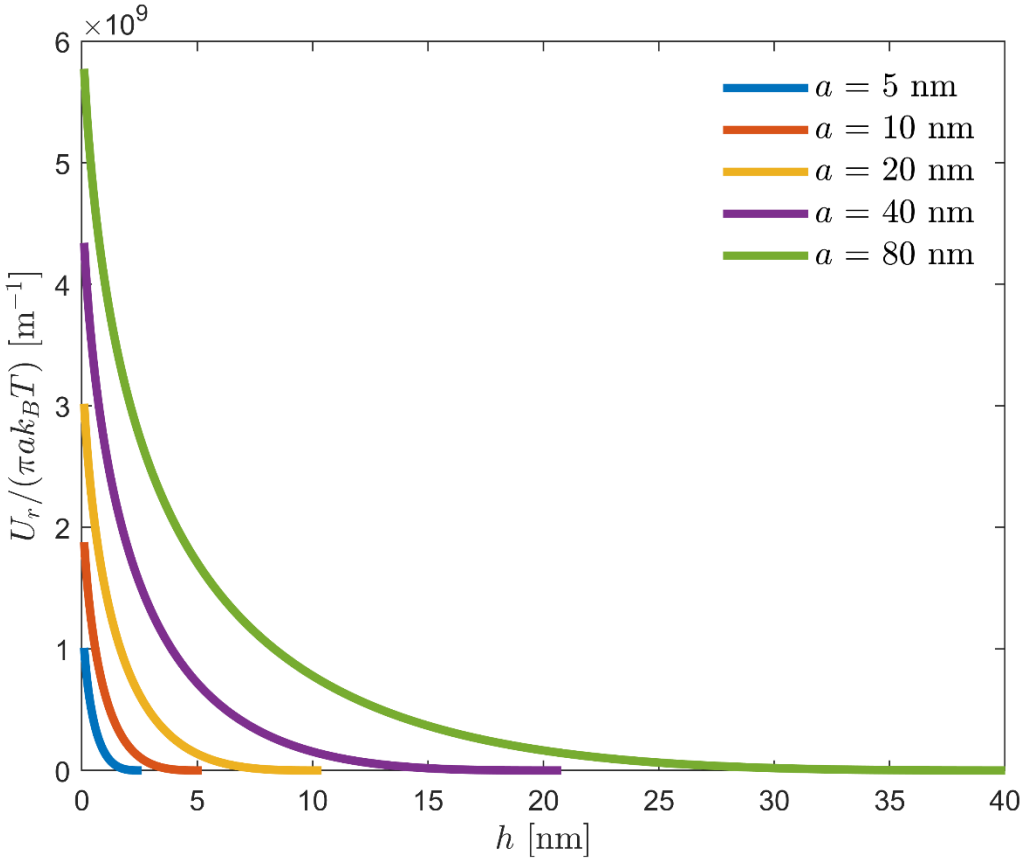

Figure 3: Radius-scaled normalized single-counterion repulsive electrostatic interaction energy between two equal-sized spheres of radius a as a function of separation distance. Ordinate is $\frac{U_r(h)}{\pi a k_B T}$ to account for the pre-factor in front of the integral in Equation 21. $\phi = 0.5$ and $q = -0.1$ C/m^2 .

Figure 4 shows the influence of surface charge density on the no-added electrolyte electrostatic interaction-potential isotherm for two different particle volume fractions and three different surface charges. As expected, larger magnitude surface charge density leads to larger repulsive interactions at both volume fractions. Surprisingly, however, the effect of surface charge density is much less pronounced than that of particle volume fraction. The reason is that C_m changes slowly compared to changes in charge density because of attenuation by the tangent function in Equation 16. These results also give some confidence to the size distribution predicted for Nafion™ aggregates in Part II[44] as the predicted sizes do not dependent strongly on q.

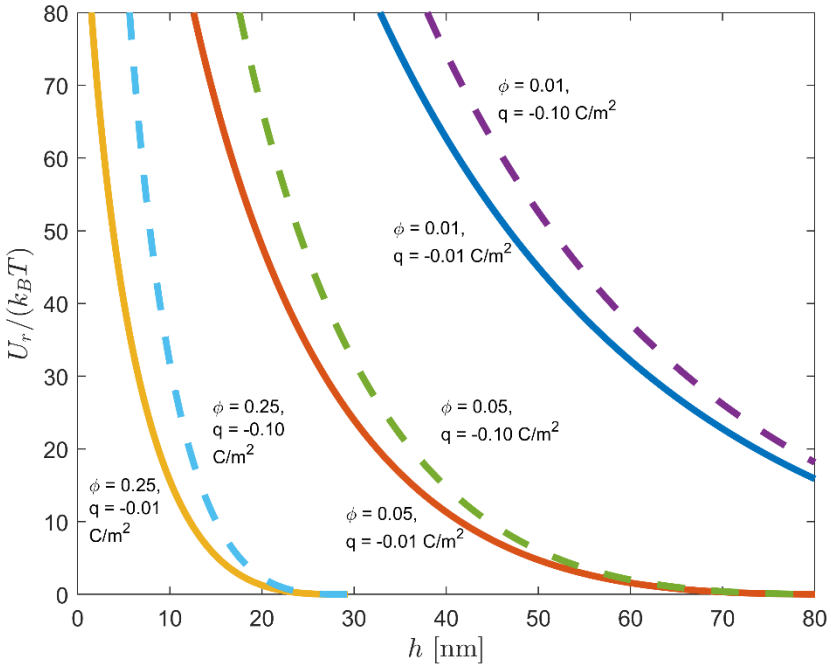

Figure 4: Normalized single-counterion repulsive electrostatic interaction energy between two equal-sized spheres ($a = 25$ nm) as a function of separation distance for varying surface charge densities and particle volume fraction.

Figure 5 contrasts the single-ion linear and nonlinear repulsive electrostatic interaction isotherms against classical 1:1 indifferent electrolyte repulsive isotherms, again both nonlinear and linear. To allow direct comparison, the background ionic strength must be specified in the classical 1:1 diffuse-double-layer interaction energies. We adopt two choices: the concentration of single counterions at L, *i.e.*, C_L, and the average concentration of single counterions in the solution, *i.e.*, $\langle C \rangle$. In analogy to solution pH, it is helpful to report these concentrations as the negative base-ten logarithm pC_L and $p\langle C \rangle$, respectively. pC_L and $p\langle C \rangle$ shorthand notations are used in Figure 5.

For a dilute dispersion of ϕ (or equivalently $L = 30$ nm), Figure 5A reveals that the nonlinear single-ion repulsive energy isotherm is closely represented by the nonlinear classic indifferent-electrolyte isotherm using C_L rather than $\langle C \rangle$. This occurs because for dilute dispersions, L is large and the counterion concentration profiles are similar in both cases. Also, the linearized Poisson-Boltzmann equation in Figure 5A overestimates the electrostatic repulsive energy relative to the nonlinear form in all cases presented. When the dispersion is more concentrated at $\phi =$

0.5787 (or equivalently $L = 5$ nm) in Figure 5B, neither comparison with the classical 1:1 electrolyte prediction gives a correct value using either pC_L or $p\langle C\rangle$ [note that when using pC notation, the unit for C is molar concentration]. In fact, deviations become significant—in some cases giving stronger repulsion from the single-ion model by a factor of two or more.

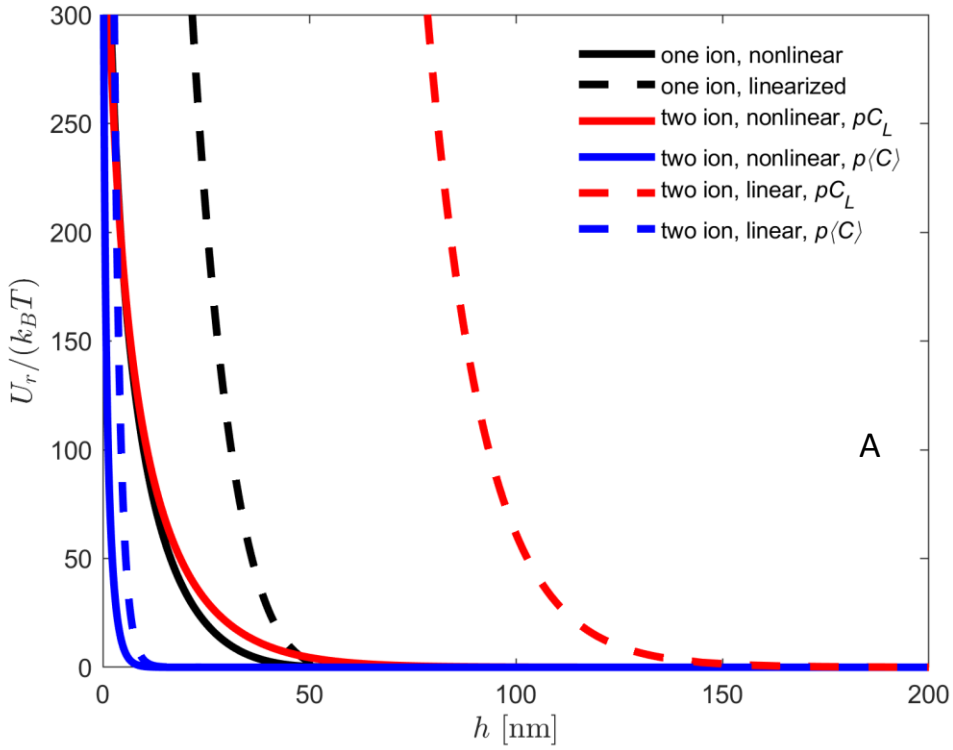

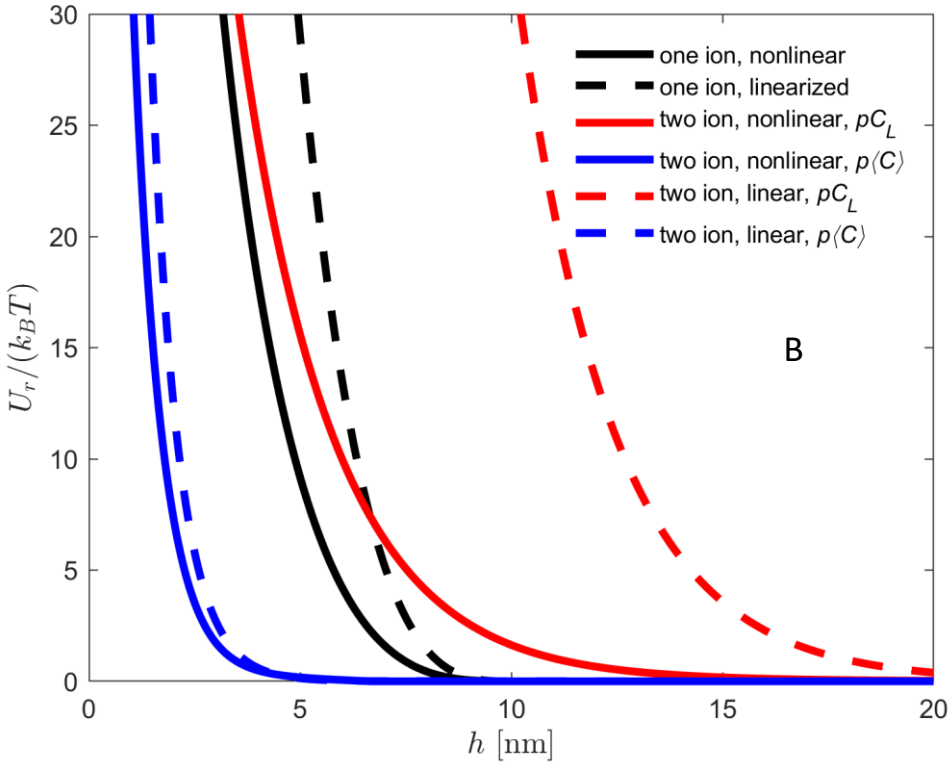

Figure 5: Normalized repulsive electrostatic interaction energy between two equal-sized spheres ($a = 25$ nm) of surface charge $q = -0.1$ C/m^2 as a function of separation distance. **A**. Comparison of dilute ($\phi = 0.094$ or $L = 30$ nm) linear and nonlinear single-counterion dispersions (one ion) with linear and nonlinear classical 1:1 indifferent electrolyte cases (two ion) with background concentrations of $p\langle C\rangle = 1.46$ and $pC_L = 3.30$. **B**. Comparison of concentrated ($\varphi = 0.5787$ or $L = 5$ nm) linear and nonlinear single-counterion dispersions (one ion) with linear and nonlinear classical 1:1 indifferent-electrolyte dispersions (two ion) with background concentrations of $p\langle C\rangle = 1.46$ and $pC_L = 3.30$.

Figure 6 reports the case previously considered in the literature of single-ion electrostatic energies for repulsion between isolated spherical particles with $C_L = 0$, thereby neglecting the backside osmotic force. [7,13–16,25] Repulsive energies are now considerably larger as seen by the enlarged ordinate scale; all single-ion potential energies displayed in Figure 5A are negligible in comparison. Thus, neglecting the backside osmotic forces leads to single-ion dispersions that do not aggregate. The linearized Poisson Boltzmann for the 1:1 indifferent-electrolyte case now

approaches the nonlinear case for large separation distances, as expected because that is the region where the linear approximation holds best. When the spheres are about to collide ($i.e., h \to 0$), however, this approximation is less accurate, and indeed, the linearized repulsive energy for the 1:1 electrolyte case increases beyond even the single-counterion repulsive energy.

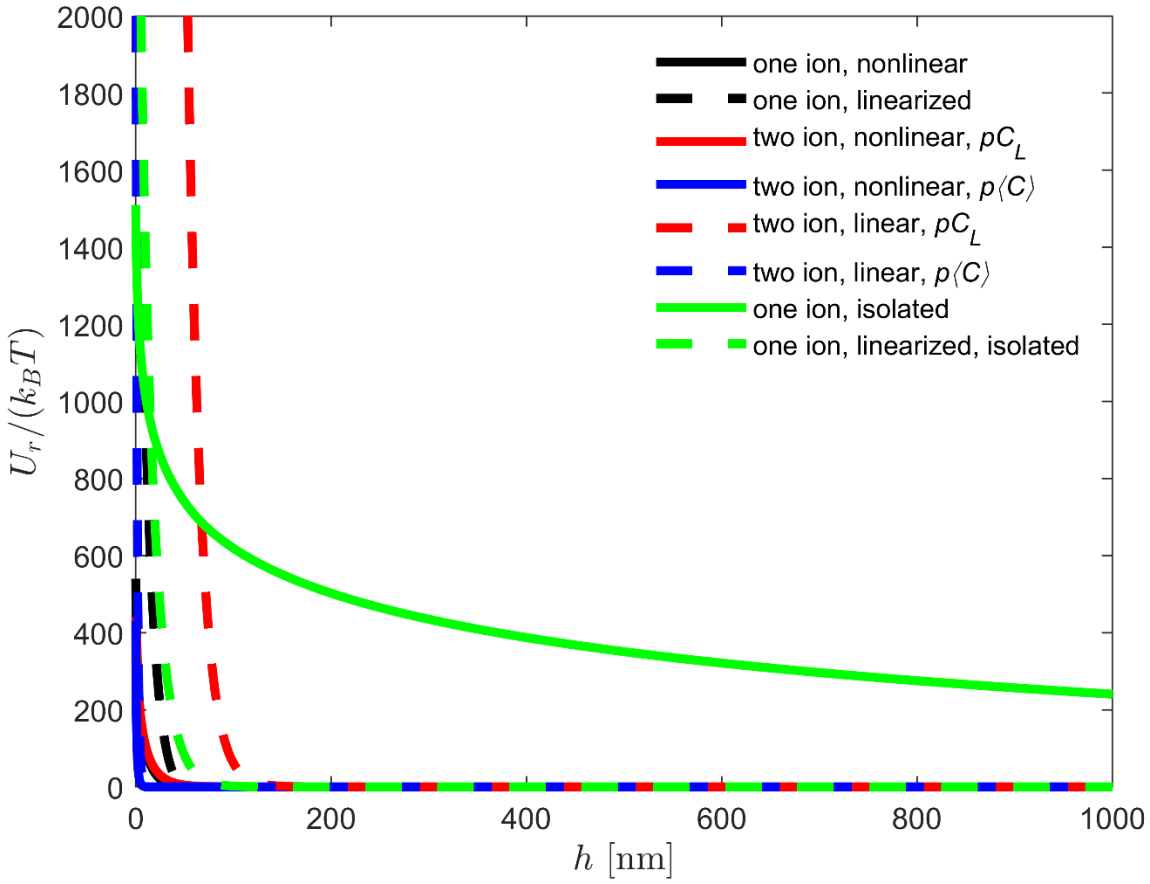

Figure 6: Normalized repulsive electrostatic interaction energy between two equal-sized spheres ($a = 25$ nm) and charge density $q = -0.1$ C/m^2 as a function of separation. Ordinate and abscissa are on expanded scales compared to Figure 5A and single-ion isolated cases (i.e., $C_L = 0$ with no background osmotic force) are included. Comparison with the nonlinear classical 1:1 indifferent electrolyte case (two ion) is with background concentrations of $p\langle C\rangle = 1.46$ and $pC_L = 3.30$. $\phi = 0.0094$ ($L = 30$ nm).

Figure 7 compares single-ion electrostatic pair potentials for particles of differing sizes. When unequal sizes are present in the dispersion, the volume-fraction partition between the two sizes must be specified. In Figure 7, we choose both sizes to have an equal volume fraction. Clearly

electrostatic repulsion increases significantly as the size of the second particle increases, partially due to the pre-integral factor in Equation 20 and partially due to increased spacings between particles with larger sizes in Equation 21. The range of sizes confirms growth instability of smaller particles and growth stability of larger particles, even when particles can only collide with those of a different size.

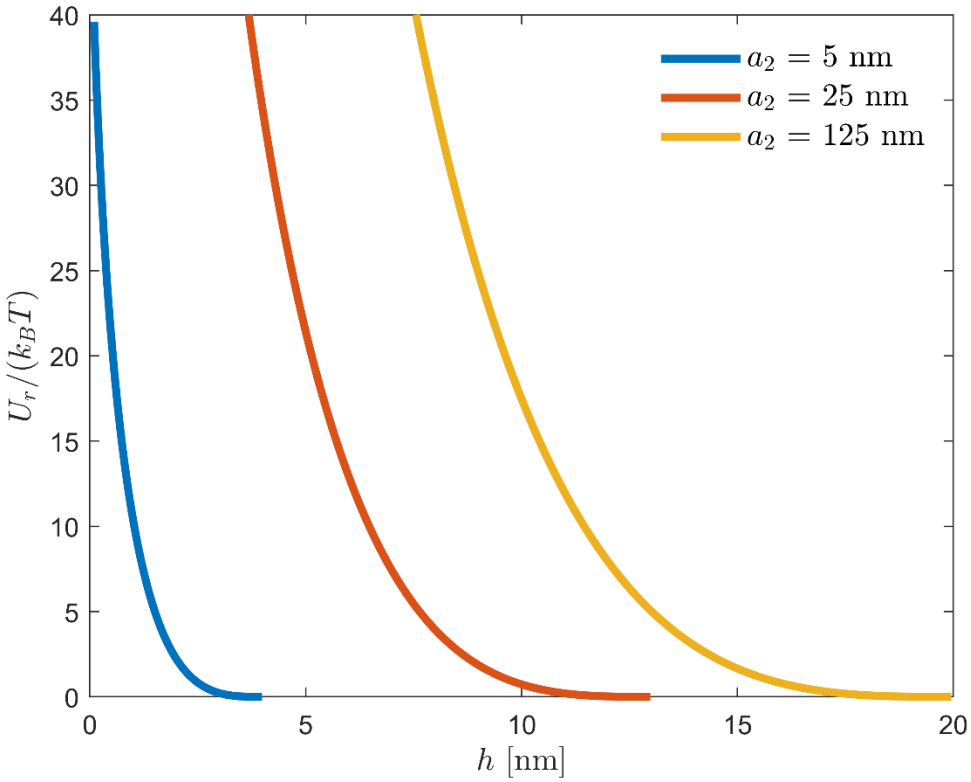

Figure 7: Normalized repulsive electrostatic interaction energy between two differently sized spheres as a function of separation. The first sphere is fixed at 25 nm and the second sphere size is varied. Each sphere size pair compared is given 50% of the total particle volume fraction. $q = -0.1\ \mathrm{C/m^2}, \phi = 0.50$, L is calculated for each pair accordingly.

Figure 8 shows the total interaction potential $U_{tot}(h)$ including Hamaker forces[8] along with the single-counterion repulsive potential energy as a function separation distance. To quantify the attractive van der Waals interaction potential, U_{vdw}, we use the well-known expression for two interacting spheres[7,8]

$$U_{vdw}(h) = -\frac{A_H}{6}\frac{a_1 a_2}{(a_1 + a_2)}\frac{1}{h} \tag{25}$$

where a_i is the radius of sphere i and the Hamaker constant A_H is taken as 10^{-19} J.[7] The dependence here on the interplay between volume fraction and size of the particles is pronounced. At the lower volume fraction in Figures 8A and 8B, neither dispersion is likely to aggregate because of the large potential-energy barriers involved. Conversely, at the higher volume fraction of 0.3 in Figures 8C and 8D, aggregation is guaranteed for the smaller particle size, but is prohibitive at the larger particle size. No effect of dispersion volume fraction is evident in the classical total pair-potential energy with added indifferent electrolyte.[5,7,9] Additionally, the importance of particle size in the no-added electrolyte total potential energy is much more pronounced than that with added indifferent salt, as noted above from Figure 3. Figure 8 accentuates the stark differences between the classical and single-ion repulsive diffuse-double-layer pair potentials and suggests that dilute no-added electrolyte dispersions are stable. By contrast, for more concentrated dispersion, small particles may aggregate whereas larger particles stabilize. This means that small particles grow until they reach a size to stabilize. This leads to the possibly of an initially unstable dispersion becoming stable by aggregating to a larger and stable particle size. In this situation, particle break-up is not necessary to achieve an unchanging particle size.

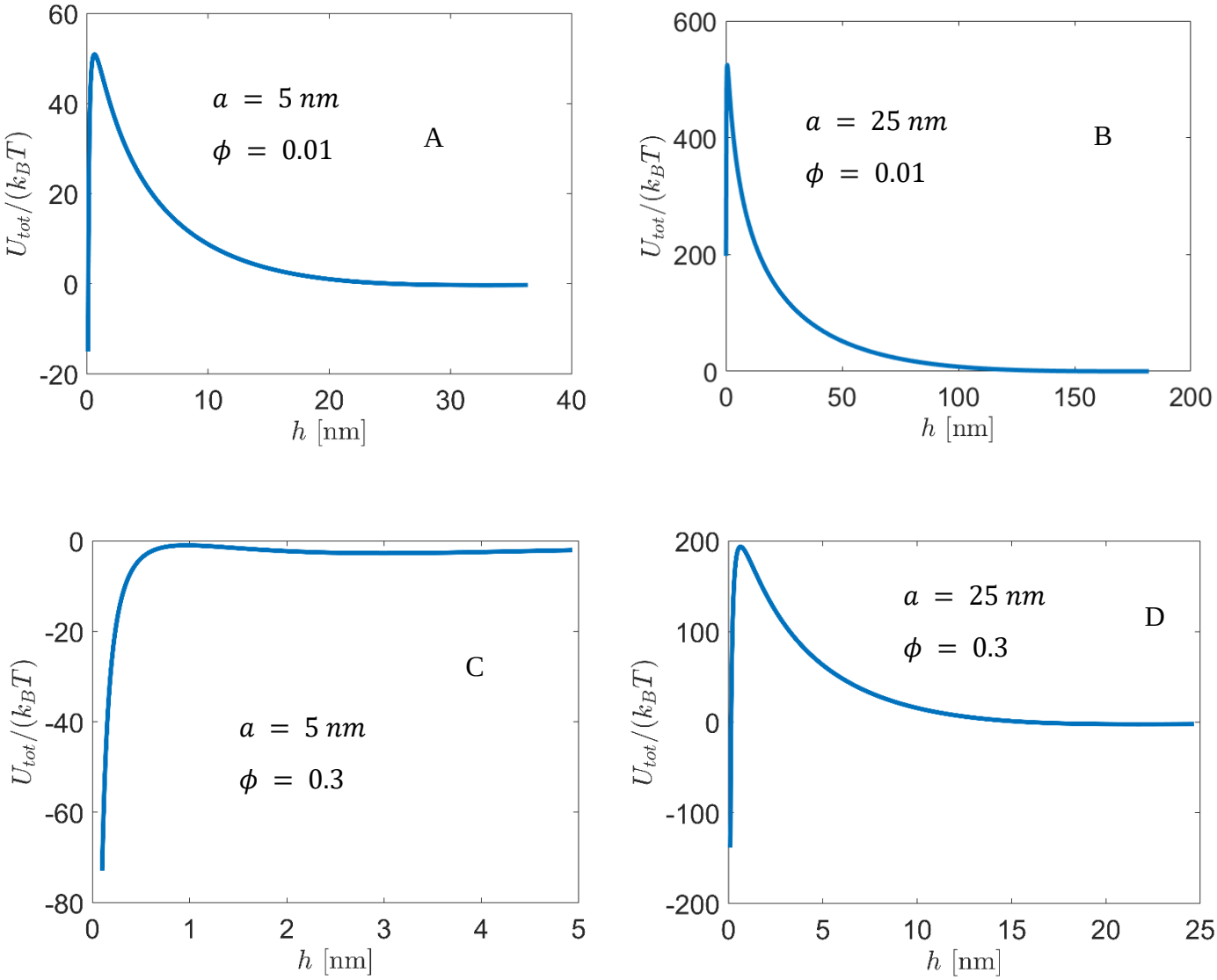

Figure 8: Normalized total interaction energies including Hamaker attractive forces between two equal-sized spheres of surface charge $q = -0.1$ C/m^2, $A_H = 10^{-19}$ J **A**. $a = 5$ nm, $\phi = 0.01$ **B**. $a = 25$ nm, $\phi = 0.01$, **C**. $a = 5$ nm, $\phi = 0.3$ **D**. $a = 25$ nm, $\phi = 0.3$.

All calculations above describe dry particles originally neutralized by an alkali monovalent cation, such as sodium ion, and immersed into an ionizing solvent containing no electrolyte. The case of particles originally in the hydrogen form, of main interest here, presents challenges because of water hydrolysis. Accordingly, hydrogen and hydroxide ions both distribute in the diffuse double

layer while maintaining water dissociation equilibrium.[46] Nonspecifically adsorbed hydroxide coions can safely be neglected in the diffuse layer because nearly all charge is neutralized by the hydrogen counterions,[5,9] especially under the acidic conditions appropriate to suspended PFSA aggregates. Likewise, specific adsorption of hydroxide ions is unlikely in acidic solutions. Nevertheless, far enough away from an anionic particle, water hydrolysis establishes electroneutrality at pH = 7, not correctly described by our single-ion double layer theory. However, if the characteristic distance necessary to achieve pH = 7 neutrality is much larger than the characteristic distance between particles, then electroneutrality is not attained. Rather, each particle encounters the diffuse layers of surrounding particles. Let λ_7 denote the traditional bulk Debye length of distilled water at $\mathrm{pH} = 7$, a value close to 1 μm, and take L as the characteristic particle separation distance. Thus, when L/λ_7 is much less than unity, water dissociation in the diffuse double layer is not important. Conversely, when L/λ_7 is larger than unity, water dissociation in the diffuse double layer becomes important and must be accounted for.[46]

Figure 9 graphs L/λ_7 as function of particle volume fraction for various average particle sizes relative to λ_7 from Equation 21. For particles sizes of 0.01 μm and below, once the suspension volume fraction attains 10^{-6} and above, pH equilibrium in the diffuse double layer may safely be neglected. As the particles become larger, accounting for water dissociation in the double layer becomes more prominent, but for particles that are hundreds of nanometers, water dissociation still does not become significant until the dispersion is above a volume fraction of 0.01.

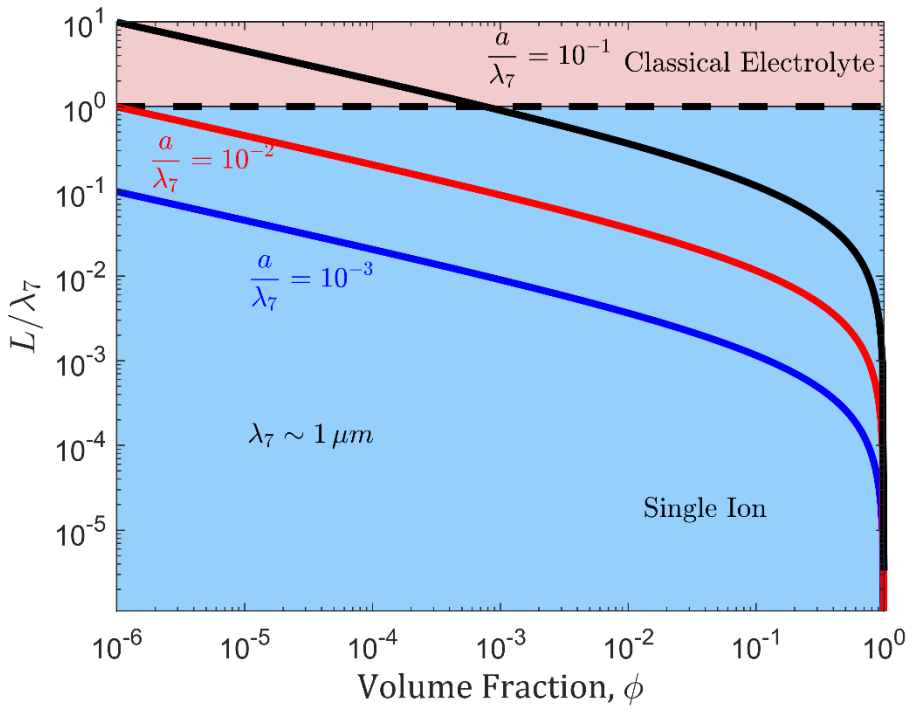

Figure 9: Normalized suspension particle separation distance relative to a pH = 7 Debye length as a function of suspension volume fraction for various normalized particle sizes. The threshold for when water dissociation becomes relevant is $\frac{L}{\lambda_7} > 1$.

The findings from Figure 9 justify the neglect of equilibrium between hydrogen and hydroxide ions in the diffuse double layer except for extremely low suspension volume fractions. Figure 10 accentuates this conclusion. The solid red line in Figure 10 graphs $pH_L = -log_{10} C_L$ (*i.e.*, using the hydronium-ion molar concentration at L) as a function of particle volume fraction. The single-ion concentration is the smallest at the characteristic distance L in the dispersion. From Figure 10, $pH_L = 7$ is not attained until the particle volume fraction is lower than 10^{-5}. For all practical particle volume fractions, there is no region of solvent electroneutrality between particles; aqueous pH equilibrium in the diffuse layer [46] can be neglected and the system considered to contain

only single hydronium ions (or single hydroxide ions if the surface charge is positive) as the sole ionic species surrounding the charged surface.

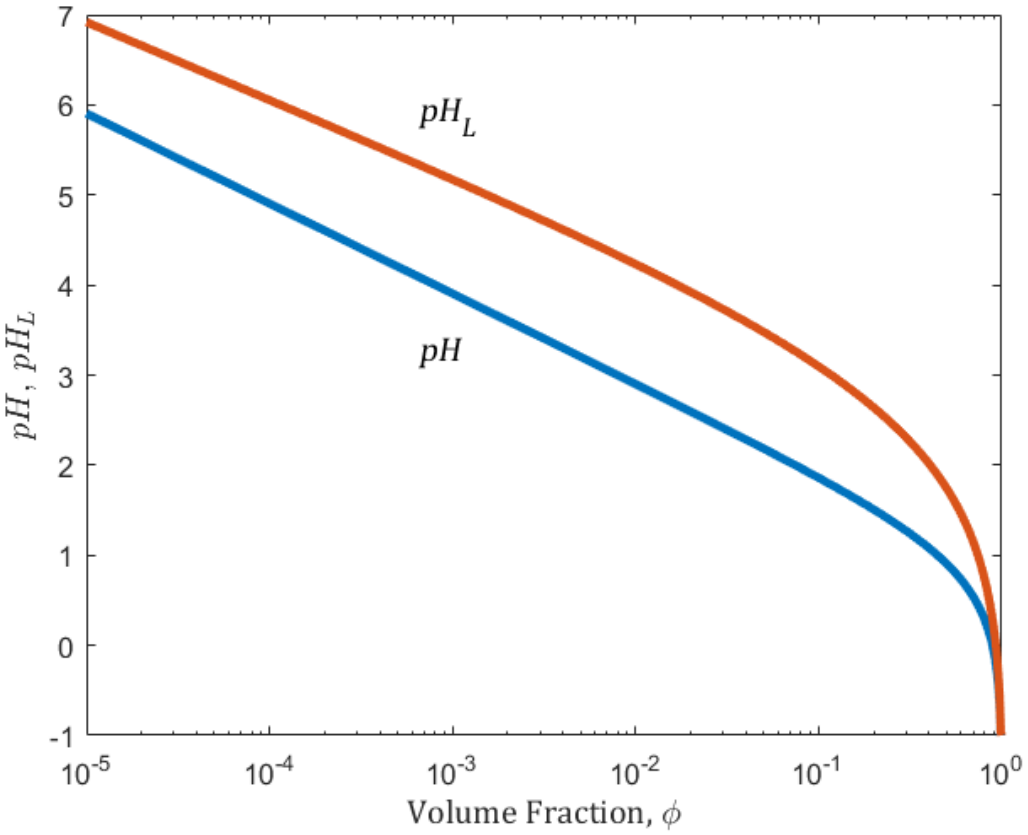

Figure 10: Predicted dispersion pH based on (blue) average hydronium ion molar concentration (pH) and (red) hydronium ion molar concentration at L (pH_L) as a semilogarithmic function of particle volume fraction. For low volume fractions, a logarithmic slope of negative unity occurs for both curves. a = 25 nm and $q = -0.1\ \mathrm{C/m^2}$.

Further, when anionic colloidal particles are originally in the hydrogen form and then immersed into a polar solvent, hydronium ions release into solution leaving behind a charged surface, and thus raising dispersion acidity.[12] The more concentrated is the dispersion solvent, the more acidic is the dispersion solvent, which has been measured using a pH probe.[17] Figure 10 also explores this observation assuming a pH probe measures the average concentration of mobile hydronium ions irrespective of their location in the diffuse double layer. The pH ordinate in Figure 10 corresponds to $\mathrm{pH} = -log_{10}\langle C\rangle$ graphed as a logarithmic function of particle volume fraction as a solid blue line, where concentration is in molar units. The constant negative unity slope at smaller volume fractions follows directly from the no-added electrolyte theory in Equation 12.

Note in Figure 10 that the no-added-electrolyte dispersions with reasonable particle size and ion-exchange capacity significantly acidify the solvent in agreement with experimental data.[17] In a 10% volume fraction, the dispersion pH falls initially from 7 to approximately 2. This effect is not present with added indifferent electrolytes, where pH neutrality is reached at the periphery of the double layer. Importantly, measurement of dispersion pH with no-added electrolyte can provide information on particle size and surface charge.[17]

Finally, the reasoning undergirding Figures 9 and 10 also provides a criterion for when classical added-electrolyte theory fails for small added-electrolyte ionic strength. Assume that the indifferent electrolyte concentration is small and below the average dissociating-ion concentration. For example, let the added 1:1 electrolyte salt be at $10^{-3}\ M$ giving a background Debye length of $\lambda_3 \sim 10\ nm$ as shown in Figure 11. When L/λ_3 in Figure 11 lies above unity, classical salt-added diffuse double layer is valid, whereas when L/λ_3 is lies below unity, single-ion diffuse double layer

theory is recommended. For direct comparison with Figure 10, the same sizes of the particles are used.

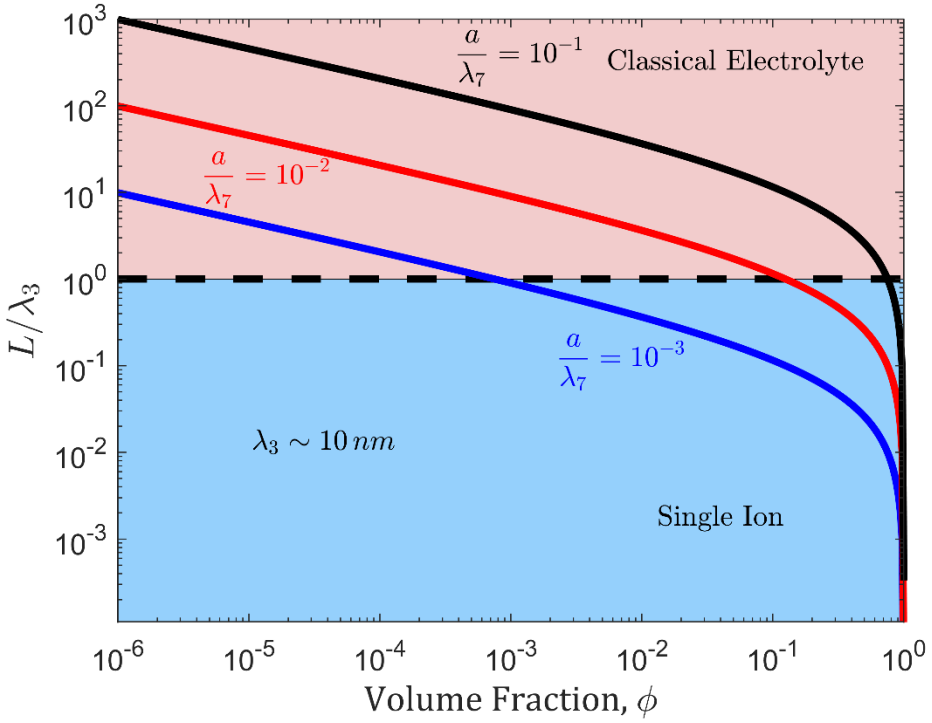

Figure 11: Normalized suspension particle separation distance relative to a $\mathrm{pH} = 3$ Debye length as a function of suspension volume fraction for various normalized particle sizes. The threshold for when classical theory becomes relevant is $\frac{L}{\lambda_3} > 1$.

Conclusions

This work addresses electrostatic colloidal-particle pair potentials for colloidal suspensions when the particle surface charge is self-neutralized by counterion dissociation/complexation release into a polar solvent. When the diffuse double layer consists only of the released surface counterions, there no longer is a neutral dispersion solvent as the solvent space-charge corona formally extends out to nearby particles specified by the colloidal volume fraction. We demonstrate that unless backside osmotic pressure is included, electrostatic repulsion is so large that all single-counterion dispersions remain stable contrary to experimental evidence.

Important and fascinating differences arise between the proposed single-counterion electrostatic repulsive potential energies and those arising in classical added-salt potential-energy theory. Deviations from the classical system include: 1) there is no region of liquid space that is electrically neutral, even in extremely low dispersion volume fraction; 2) the electrostatic pair potentials in single-counterion theory depend strongly on particle volume fraction: the smaller is the particle volume fraction the larger is the repulsive pair potential; 3) the single-ion potential energy exhibits a much stronger size dependence than does classical added-electrolyte potential (see Figure 3); 4) Single-ion net electrostatic repulsion between interacting particles is reduced by the presence of nearby surrounding particles. That is, the single-ion electrostatic potential energy is inherently multibody; and 5) single-ion potentials are much larger than the corresponding added-electrolyte potential energies for the same separation distances (see Figures 5 and 6). This behavior means that size distributions for aggregating particles in the single-ion case are much smaller. All these differences arise from including the counterion concentration at the characteristic distance L in the Derjaguin repulsive-energy expression and solving for this concentration given the surface charge density. L describes the average spacing between particles calculated from the suspension volume fraction.

The strong dependences of the single-ion electrostatic pair potential on particle size and volume fraction lead to intriguing behavior not appearing in classical DLVO theory. Keeping all else constant, dispersions stable at low volume fraction can become unstable at high volume fraction. Moreover, a non-zero volume fraction dispersion of small particles can be unstable but stabilize at larger aggregate size. This means that a no-added electrolyte dispersion of unstable fine particles can coarsen to a stable dispersion of larger irreversibly attached aggregates. We also find that no-added electrolyte dispersions of realistic particle size and volume fraction greatly acidify a suspending solvent. Dispersion pH is predicted to fall substantially initially from 7 to 2 even at only 10% particle volume fraction for the charge density assumed. The proposed single-counterion electrostatic pair potential theory provides a new powerful tool to understand dispersion colloidal behavior when surface charge arises solely from dissociate/desorption of surface ionogenic groups or ion-exchange sites. In Part II, the developed single-ion potential energies are utilized to predict successfully size distributions of Nafion™ PFSA aggregates and the resulting suspension *pH* of n-propanol/water solutions as a function of volume fraction.[44] Classical DLVO electrostatic potential

energies for added electrolyte, which are independent of suspension volume fraction, fail in this endeavor.

Supporting Information. Numerical details and derivation of linearized potentials.

Acknowledgements

This work was supported by the Hydrogen and Fuel Cell Technologies Office (HFTO), Office of Energy Efficiency and Renewable Energy, U.S. Department of Energy (DOE) through the Million Mile Fuel Cell Truck (M2FCT) consortia, technology managers G. Kleen and D. Papageorgopoulos, under Contract Number DE-AC02-05CH11231.

Nomenclature

a	Radius of sphere [m]
A_H	Hamaker Constant [J]
C_∞	Number concentration of counterions far from the surface $[1/\mathrm{m}^3]$
C_L	Number concentration of counterions per solvent volume at L $[1/m^3]$
C_m	Midpoint number concentration of counterions per solvent volume between two flat plates $[1/m^3]$
$\langle C \rangle$	Average number counterion concentration $[1/\mathrm{m}^3]$
DLVO	Derjaguin-Landau-Verwey-Overbeek
ϵ	Fluid dielectric permittivity $[\mathrm{C}^2/\mathrm{N}^2 \cdot \mathrm{m}]$
h	Separation distance between two flat plates
k_B	Boltzmann constant (1.38×10^{-23} J/K)
L	Dissociation distance of counterions away from a flat plate [m]
λ	Debye length [m]
P	Osmotic pressure [Pa]
pC_L	Log normalized counterion molar concentration at L $(-log_{10}C_L)$
pH	Log normalized average proton molar concentration $(-log_{10}\langle C \rangle)$
pH_L	Log normalized proton molar concentration at L $(-log_{10}C_L)$
ϕ	Volume fraction of particles

Φ	Potential [V]
q	Surface charge density $[\mathrm{C/m^2}]$
R	Ideal gas constant $(8.314\ \mathrm{J/mol \cdot K})$
T	Temperature [K]
x	Distance from flat plate [m]
U_r	Repulsive energy between two spheres [J]
U_{vdw}	Attractive van-der-Waals energy between two spheres [J]
V_R	Repulsive energy per unit area for two flat plates $[\mathrm{J/m^2}]$
z	Charge number

References

(1) Conde, J. J.; Ferreira-Aparicio, P.; Chaparro, A. M. Electrospray Deposition: A Breakthrough Technique for Proton Exchange Membrane Fuel Cell Catalyst Layer Fabrication. *ACS Appl. Energy Mater.* **2021**, *4* (8), 7394–7404. https://doi.org/10.1021/acsaem.1c01445.

(2) Liu, H.; Ney, L.; Zamel, N.; Li, X. Effect of Catalyst Ink and Formation Process on the Multiscale Structure of Catalyst Layers in PEM Fuel Cells. *Applied Sciences* **2022**, *12* (8), 3776. https://doi.org/10.3390/app12083776.

(3) Bapat, S.; Giehl, C.; Kohsakowski, S.; Peinecke, V.; Schäffler, M.; Segets, D. On the State and Stability of Fuel Cell Catalyst Inks. *Advanced Powder Technology* **2021**, *32* (10), 3845–3859. https://doi.org/10.1016/j.apt.2021.08.030.

(4) Zhang, H.; Wang, X.; Zhang, J.; Zhang, J. Conventional Catalyst Ink, Catalyst Layer and MEA Preparation. In *PEM Fuel Cell Electrocatalysts and Catalyst Layers: Fundamentals and Applications*; Zhang, J., Ed.; Springer: London, 2008; pp 889–916. https://doi.org/10.1007/978-1-84800-936-3_19.

(5) Kruyt, Hugor. Electrochemistry of the Double Layer. In *Colloid Science. Volume 1: Irreversible Systems*; Elsevier Publishing Company, 1952; Vol. 1, pp 115–146.

(6) Marmur, A. A Kinetic Theory Approach to Primary and Secondary Minimum Coagulations and Their Combination. *Journal of Colloid and Interface Science* **1979**, *72* (1), 41–48. https://doi.org/10.1016/0021-9797(79)90178-4.

(7) Israelachvili, J. N. Electrostatic Forces between Surfaces in Liquids. In *Intermolecular and Surface Forces*; Elsevier, 2011; pp 291–340. https://doi.org/10.1016/B978-0-12-375182-9.10014-4.

(8) Shukla, S.; Bhattacharjee, S.; Weber, A. Z.; Secanell, M. Experimental and Theoretical Analysis of Ink Dispersion Stability for Polymer Electrolyte Fuel Cell Applications. *J. Electrochem. Soc.* **2017**, *164* (6), F600–F609. https://doi.org/10.1149/2.0961706jes.

(9) Berg, J. C. Kinetics of Aggregation. In *An Introduction to Interfaces and Colloids: The Bridge to Nanoscience*; World Scientific, 2009; pp 560–582. https://doi.org/10.1142/7579.
(10) Muneer, R.; Hashmet, M. R.; Pourafshary, P. Fine Migration Control in Sandstones: Surface Force Analysis and Application of DLVO Theory. *ACS Omega* **2020**, *5* (49), 31624–31639. https://doi.org/10.1021/acsomega.0c03943.
(11) Vilinska, A.; Rao, K. H. Surface Thermodynamics and Extended DLVO Theory of Acidithiobacillus Ferrooxidans Cells Adhesion on Pyrite and Chalcopyrite. *TOCOLLSJ* **2009**, *2* (1), 1–14. https://doi.org/10.2174/1876530000902010001.
(12) Newman, J.; Thomas-Alyea, K. E. *Electrochemical Systems*; John Wiley & Sons, 2004.
(13) Cowley, A. C.; Fuller, N. L.; Rand, R. P.; Parsegian, V. A. Measurement of Repulsive Forces between Charged Phospholipid Bilayers. *Biochemistry* **1978**, *17* (15), 3163–3168. https://doi.org/10.1021/bi00608a034.
(14) Chang, S. H. Electrostatic Interaction between Dissimilarly Charged Membranes in Salt-Free Solution. *AMM* **2014**, *590*, 224–228. https://doi.org/10.4028/www.scientific.net/AMM.590.224.
(15) Chang, S.-H. Electric Double-Layer Forces between Dissimilarly Charged Planar Surfaces in Salt-Free Solution. *Procedia Engineering* **2014**, *79*, 318–322. https://doi.org/10.1016/j.proeng.2014.06.349.
(16) Briscoe, W. H.; Attard, P. Counterion-Only Electrical Double Layer: A Constrained Entropy Approach. *J. Chem. Phys.* **2002**, *117* (11), 5452–5464. https://doi.org/10.1063/1.1500359.
(17) Berlinger, S. A.; McCloskey, B. D.; Weber, A. Z. Inherent Acidity of Perfluorosulfonic Acid Ionomer Dispersions and Implications for Ink Aggregation. *J. Phys. Chem. B* **2018**, *122* (31), 7790–7796. https://doi.org/10.1021/acs.jpcb.8b06493.
(18) Mabuchi, T.; Huang, S.-F.; Tokumasu, T. Nafion Ionomer Dispersion in Mixtures of 1-Propanol and Water Based on the Martini Coarse-Grained Model. *J Polymer Science* **2020**, *58* (3), 487–499. https://doi.org/10.1002/pol.20190101.
(19) Mabuchi, T.; Huang, S.-F.; Tokumasu, T. Dispersion of Nafion Ionomer Aggregates in 1-Propanol/Water Solutions: Effects of Ionomer Concentration, Alcohol Content, and Salt Addition. *Macromolecules* **2020**, *53* (9), 3273–3283. https://doi.org/10.1021/acs.macromol.9b02725.
(20) Silva, R. F.; De Francesco, M.; Pozio, A. Solution-Cast Nafion® Ionomer Membranes: Preparation and Characterization. *Electrochimica Acta* **2004**, *49* (19), 3211–3219. https://doi.org/10.1016/j.electacta.2004.02.035.
(21) Tarokh, A.; Karan, K.; Ponnurangam, S. Atomistic MD Study of Nafion Dispersions: Role of Solvent and Counterion in the Aggregate Structure, Ionic Clustering, and Acid Dissociation. *Macromolecules* **2020**, *53* (1), 288–301. https://doi.org/10.1021/acs.macromol.9b01663.
(22) Yamaguchi, M.; Terao, T.; Ohira, A.; Hasegawa, N.; Shinohara, K. Size and Shape of Nafion Particles in Water after High-Temperature Treatment. *J Polymer Science Part B: Polymer Physics* **2019**, *57* (13), 813–818. https://doi.org/10.1002/polb.24833.
(23) Wang, Q.; Eikerling, M.; Song, D.; Liu, Z.-S. Modeling of Ultrathin Two-Phase Catalyst Layers in PEFCs. *J. Electrochem. Soc.* **2007**, *154* (6), F95. https://doi.org/10.1149/1.2716557.
(24) Chan, K.; Eikerling, M. A Pore-Scale Model of Oxygen Reduction in Ionomer-Free Catalyst Layers of PEFCs. *J. Electrochem. Soc.* **2010**, *158* (1), B18. https://doi.org/10.1149/1.3505042.

(25) Engstrom, S.; Wennerstrom, H. Ion Condensation on Planar Surfaces. A Solution of the Poisson-Boltzmann Equation for Two Parallel Charged Plates. *J. Phys. Chem.* **1978**, *82* (25), 2711–2714. https://doi.org/10.1021/j100514a017.
(26) Alexander, S.; Chaikin, P. M.; Grant, P.; Morales, G. J.; Pincus, P.; Hone, D. Charge Renormalization, Osmotic Pressure, and Bulk Modulus of Colloidal Crystals: Theory. *The Journal of Chemical Physics* **1984**, *80* (11), 5776–5781. https://doi.org/10.1063/1.446600.
(27) Bocquet, L.; Trizac, E.; Aubouy, M. Effective Charge Saturation in Colloidal Suspensions. *The Journal of Chemical Physics* **2002**, *117* (17), 8138–8152. https://doi.org/10.1063/1.1511507.
(28) Ryoo, W.; Webber, S. E.; Bonnecaze, R. T.; Johnston, K. P. Long-Ranged Electrostatic Repulsion and Crystallization of Emulsion Droplets in an Ultralow Dielectric Medium Supercritical Carbon Dioxide. *Langmuir* **2006**, *22* (3), 1006–1015. https://doi.org/10.1021/la052298i.
(29) SenGupta, A. K.; Papadopoulos, K. D. Stability of Concentrated Colloids: The Controlling Parameters. *Journal of Colloid and Interface Science* **1998**, *203* (2), 345–353. https://doi.org/10.1006/jcis.1998.5524.
(30) Russel, W. B.; Saville, D. A.; Schowalter, W. R. Equilibrium Phase Behavior. In *Colloidal Dispersions*; Cambridge Monographs on Mechanics; Cambridge University Press: Cambridge, 1989; pp 329–365. https://doi.org/10.1017/CBO9780511608810.
(31) Hachisu, S.; Kobayashi, Y.; Kose, A. Phase Separation in Monodisperse Latexes. *Journal of Colloid and Interface Science* **1973**, *42* (2), 342–348. https://doi.org/10.1016/0021-9797(73)90298-1.
(32) Pieranski, P. Colloidal Crystals. *Contemporary Physics* **1983**, *24* (1), 25–73. https://doi.org/10.1080/00107518308227471.
(33) Reiner, E. S.; Radke, C. J. Electrostatic Interactions in Colloidal Suspensions: Tests of Pairwise Additivity. *AIChE Journal* **1991**, *37* (6), 805–824. https://doi.org/10.1002/aic.690370604.
(34) Wennerström, H. Electrostatic Interactions in Concentrated Colloidal Dispersions. *Phys. Chem. Chem. Phys.* **2017**, *19* (35), 23849–23853. https://doi.org/10.1039/C7CP02594G.
(35) Kralchevsky, P. A.; Danov, K. D.; Petkov, P. V. Soft Electrostatic Repulsion in Particle Monolayers at Liquid Interfaces: Surface Pressure and Effect of Aggregation. *Philosophical Transactions of the Royal Society A: Mathematical, Physical and Engineering Sciences* **2016**, *374* (2072), 20150130. https://doi.org/10.1098/rsta.2015.0130.
(36) Briscoe, W. H.; Horn, R. G. Direct Measurement of Surface Forces Due to Charging of Solids Immersed in a Nonpolar Liquid. *Langmuir* **2002**, *18* (10), 3945–3956. https://doi.org/10.1021/la015657s.
(37) Attard, P. Electrostatic Fluctuation and Double Layer Interactions between Surfaces. PhD Thesis, Australian National University, 1988.
(38) Ruiz-Cabello, F. J. M.; Moazzami-Gudarzi, M.; Elzbieciak-Wodka, M.; Maroni, P.; Labbez, C.; Borkovec, M.; Trefalt, G. Long-Ranged and Soft Interactions between Charged Colloidal Particles Induced by Multivalent Coions. *Soft Matter* **2015**, *11* (8), 1562–1571. https://doi.org/10.1039/C4SM02510E.
(39) Clarke, D. R.; Shaw, T. M.; Philipse, A. P.; Horn, R. G. Possible Electrical Double-Layer Contribution to the Equilibrium Thickness of Intergranular Glass Films in Polycrystalline

Ceramics. *Journal of the American Ceramic Society* **1993**, *76* (5), 1201–1204. https://doi.org/10.1111/j.1151-2916.1993.tb03741.x.
(40) Ohshima, H. Electrostatic Interaction between Ion-Penetrable Membranes in a Salt-Free Medium. *J Colloid and Interface Science* **2003**, *260* (2), 339–343. https://doi.org/10.1016/S0021-9797(02)00159-5.
(41) Wennerström, H.; Stenhammar, J. Derivation of the Derjaguin Approximation for the Case of Inhomogeneous Solvents. *J. Chem. Phys.* **2020**, *152* (23), 234704. https://doi.org/10.1063/5.0011446.
(42) Sengupta, A. K.; Papadopoulos, K. D. Electrical Double-Layer Interaction between Two Eccentric Spherical Surfaces. *Journal of Colloid and Interface Science* **1992**, *149* (1), 135–152. https://doi.org/10.1016/0021-9797(92)90399-7.
(43) Sonnefeld, J.; Göbel, A.; Vogelsberger, W. Surface Charge Density on Spherical Silica Particles in Aqueous Alkali Chloride Solutions. *Colloid Polym Sci* **1995**, *273* (10), 926–931. https://doi.org/10.1007/BF00660369.
(44) Srivastav, H.; Weber, A. Z.; Radke, C. J. Colloidal Stability of PFSA-Ionomer Dispersions Part II: Determination of Suspension PH Using Single-Ion Potential Energies, In Review. *Langmuir* **2023**.
(45) Ngo, T. T.; Yu, T. L.; Lin, H.-L. Influence of the Composition of Isopropyl Alcohol/Water Mixture Solvents in Catalyst Ink Solutions on Proton Exchange Membrane Fuel Cell Performance. *Journal of Power Sources* **2013**, *225*, 293–303. https://doi.org/10.1016/j.jpowsour.2012.10.055.
(46) Chamberlayne, C. F.; Zare, R. N.; Santiago, J. G. Effects of Weak Electrolytes on Electric Double Layer Ion Distributions. *J. Phys. Chem. Lett.* **2020**, *11* (19), 8302–8306. https://doi.org/10.1021/acs.jpclett.0c02247.

TOC Graphic